





## 32 1. Introduction

33 In recent decades, the eutrophication of water body driven by excess nutrient loads from lands due to human  
34 activities is increasing year by year, which leads to an enhancement of hypoxic zone (Murphy et al., 2011;  
35 Rabouille et al., 2008). Dissolved oxygen (DO) threatens marine animals when its concentration is lower than 2  
36 mg/L or 62.5  $\mu\text{mol/L}$ , which is defined as hypoxia (Diaz, 2001; H Wei et al., 2007). When DO is less than 2.0  
37 mg/L, the majority of marine aquatic organisms will be dead, especially benthic animal (Karlson et al., 2002).  
38 Hypoxia is one of the most severe environmental issues affecting estuarine and coastal marine ecosystems around  
39 the world. Hypoxia can reduce the diversity of marine species, change the community structure of marine  
40 organisms, reduce the richness of fish and benthic animals, and thus affect the fishery production and bring about  
41 direct or indirect economic loss (Yin et al., 2004).

42 The hypoxia off Yangtze Estuary was first found in 1959 (Gu, 1980). In recent years, with the increase of  
43 global warming and pollutant emissions, the hypoxic area off Yangtze Estuary expanded fast and became one of  
44 world's largest costal hypoxia (Vaquer-Sunyer and Duarte, 2008). In the 1950s, the occurrence probability on  
45 hypoxia off Yangtze Estuary in summer was 60%, while after 1990s hypoxia occurrence probability reached 90%,  
46 and hypoxic areas which were greater than 5000  $\text{km}^2$  basically occurred after the end of 1990s (Wang, 2009).

47 The formation of hypoxia adjacent to the Yangtze Estuary is a complex process, which is the result of both  
48 physical and biochemical processes. Previous research had shown that the formation and evolution of hypoxia  
49 were closely related to river discharge, Taiwan Warm Current, wind speed, wind direction, bottom topography,  
50 and the degradation of organic (Li et al., 2011; Ning et al., 2011; Wang, 2009; X Li, 2011; Zhou F, 2010; Zhu et al.,  
51 2011). It was generally accepted that the increase in hypoxic extent was mainly driven by the rising anthropogenic  
52 nutrient inputs from the Yangtze River. However many studies had indicated that the physical factors have  
53 important contributions to the formation of the annual variation of hypoxia. Wilson et al. (2008) found that the  
54 wind-driven circulation had an important influence on the West Long Island Strait stratification and vertical  
55 mixing. When the wind direction changed in summer, it prevented the exchange of dissolved oxygen from the  
56 bottom to surface, which made the West Long Island Strait appear hypoxia. Through numerical simulation,  
57 Obenour (2015) found that the river nutrient concentration was very important for the formation of hypoxia.  
58 However the stratification, which presented as a function of river discharge, wind speed and wind direction,  
59 contributed to a larger extent to the interannual variability in hypoxia. Due to the limitation of observation data, it  
60 was difficult to fully understand the temporal and spatial variation of hypoxia, and quantitatively described the  
61 influence of physical factors on the hypoxia off the Yangtze Estuary. In this paper, a three-dimensional  
62 hydrodynamic model (Regional Ocean Model System, ROMS) coupled nitrogen cycle model described by Fennel



63 et al. (2006) were used to simulate ecosystem of the East China Sea. Through this coupled model, the effects of  
64 river discharge, wind speed and wind direction on dissolved oxygen at sublayer and bottom of sea waters off the  
65 Yangtze Estuary were analyzed quantitatively.

66

## 67 **2. Model description**

### 68 **2.1 Physical model**

69 The physical circulation model used in this study was based on the Regional Ocean Model System, which  
70 was a free-surface, terrain-following, primitive equations ocean model (Haidvogel et al., 2008; Shchepetkin A F,  
71 2005). This model was built for the East China Sea (114-143°E, 22.3-53.1°N) with a 1/15 degree horizontal  
72 resolution and 30 vertical layers (Fig. 1a). The models' terrain-following vertical layers were stretched to result in  
73 increased resolution near the surface and bottom. A fourth-order horizontal advection scheme for tracers, a  
74 third-order mixing by Mellor and Yamad were used in the model (Mellor G 1982). At the offshore open boundary,  
75 we employed Chapman's condition for surface elevation (Chapman, 1985), Flather's condition for barotropic  
76 velocity (Flather, 1976), and a combination of radiation condition and nudging for tracers (Marchesiello et al.,  
77 2001).

78 The model was initialized with climatological temperature, salinity from the Generalized Digital  
79 Environment Model (GDEM). The south, north and east of the pattern were open boundary, and the west was  
80 closed boundary. On the open boundary, the average profile of temperature, salinity and sea level were derived  
81 from Simple Ocean Data Assimilation (SODA). The model was forced with net heat flux, fresh water flux, short  
82 wave radiation, wind stress and so on, which derived from NCEP/CFSR reanalysis. In the model, the runoff of the  
83 Yangtze River was determined by the month average discharge of the Datong station (Liu Xincheng, 2002).

### 84 **2.2 Biological model**

85 The biological module was based on the nitrogen cycle model described in the study by Fennel et al. (2006).  
86 The model included ten state variables: two species of dissolved inorganic nitrogen (nitrate,  $\text{NO}_3$  and ammonium,  
87  $\text{NH}_4$ ), one phytoplankton group, one zooplankton group, chlorophyll-a, two species detritus representing large,  
88 fast-sinking particles and suspended, small particles, and oxygen, total inorganic carbon, alkalinity. The source of  
89 dissolved oxygen in the model was air-sea gas exchange, primary production, and the sink included the  
90 respiration zooplankton, nitrification, decomposing detritus and sediment oxygen consumption(Fennel et al.,  
91 2013). At the sediment-water interface, the model assumed "instantaneous remineralization" by which organic  
92 matter that sank to the bottom was remineralized immediately to ammonium and oxygen was taken up



93 immediately as well. The initial fields and boundary conditions for the biological tracers were derived from the  
94 World Ocean Atlas 2009 (WOA2009). The initial value of ammonium was set to  $1\text{mmol/m}^3$ . The chlorophyll-a  
95 concentration was extrapolated in the vertical direction from surface values specified by SeaWiFS monthly  
96 climatological data and the extrapolation was based on the generalized Gaussian curve of typical pigment profile  
97 (Lewis et al., 1983; Morel and Berthon, 1989). The initial values of phytoplankton, zooplankton and detritus  
98 concentrations were set to 0.5, 0.25 and 0.25 times of chlorophyll-a concentration, respectively. Ammonium can  
99 be rapidly nitrified into nitrate at the inner estuaries. Therefore, only nitrate discharged from the Yangtze River  
100 was considered in the model.

101 After the physical model had spun-up for 10 year since climatological 1st January, the coupled  
102 physical-biological model was simulated from 1st January 2006 to 31th December 2010. A series of numerical  
103 experiments in 2010 were set up to study the influence of river discharge, wind speed and wind direction on  
104 hypoxia adjacent to the Yangtze Estuary.

105

### 106 **3. Results**

#### 107 **3.1. Model validation**

108 The comparison of sea surface temperature (SST) and sea surface salinity (SSS) in August between model  
109 and GDEM were shown in Fig. 2. Apparently, the model results of SST and SSS were similar to GDEM data. The  
110 spatial distribution characteristic of SST was gradually increasing from north to south. The model results of the  
111 SST along the coastal waters were higher than GDEM data, especially offshore of Bohai and the Yellow Sea. In  
112 August, under the control of southerly wind, the Yangtze diluted water expanded to the northeast direction. From  
113 the difference of SSS between simulated results and GDEM data, we found that a certain deviation between them  
114 near the Yangtze Estuary. In reality, the GDEM data was not very accurate along the China coast, due to its low  
115 spatial resolution. The distributions of SSS in our model were comparable to the results conducted by Liu et al.  
116 (2010).

117 Fig. 3a,3b showed that the comparison of sea surface chlorophyll-a concentration between the model results  
118 and SeaWiFS-derived data in August. It can be seen that the patterns of chlorophyll-a were comparable to the  
119 SeaWiFS-derived data. For example, the distribution of chlorophyll-a was extended to northeast in summer. The  
120 chlorophyll-a concentration was  $5\text{-}10\text{mg/m}^3$  in surface waters adjacent to the Changjiang Estuary, then decreased  
121 rapidly eastward to the open shelf, where values were  $0.1\text{-}0.5\text{mg/m}^3$ . The modeled chlorophyll-a values in the  
122 inner and mid shelves were quite close to the SeaWiFS-derived data, while the model generally underestimated  
123 the chlorophyll-a in the outer shelf. Compared with the SeaWiFS-derived data, the concentration of chlorophyll in



124 the south of 28°N was also lower. This was mainly due to only consider the nutrient inputs from the Yangtze River  
125 in the model.

126 In-situ nitrate and ammonium distributions along section 30°N (see Fig. 3) in August were used to evaluate  
127 the simulation capability of biological model. Both in-situ and model nitrate distributions showed that the  
128 presence of relative high nitrate in the bottom (>4 mmol/m<sup>3</sup>), but low (< 2 mmol/m<sup>3</sup>) in the surface. An analogous  
129 structure was present in the in-situ temperature and salinity distributions located between 123°E and 124°E  
130 reported by Wang (2009), so that upwelled water inside the trough involved not only low temperature and high  
131 salinity but also high nutrients. From the Fig. 3c,3d, a definite deviation between the model and in situ data can be  
132 seen. The high nitrate concentration appeared above water layers of 25 meter along the section of 123°E, but the  
133 model failed to reproduce it. The underestimation probably resulted from the insufficient dispersion of high nitrate,  
134 which was source from Yangtze river diluted water. Along the section of 30°N, the patterns of model ammonium  
135 resembled that of observations. Ammonium was relatively high in the near-shore waters (>2 mmol/m<sup>3</sup>), then  
136 decreased toward the open waters (<1 mmol/m<sup>3</sup>). An obvious high-concentration area was located between 123°E  
137 and 124°E, which reconfirmed that the Taiwan warm upwelling brought the bottom water with high nutrients to  
138 the surface.

139 Fig. 4 showed the comparison between in-situ and model results of dissolved oxygen and nitrate  
140 concentration at the stations (see Fig.1c). It can be seen that the simulated dissolved oxygen and nitrate resembled  
141 the in-situ data. The root mean square error of RMS on surface dissolved oxygen, bottom dissolved oxygen,  
142 surface nitrate and bottom nitrate were 0.55, 0.56, 1.58 and 1.94 respectively. The concentration of dissolved  
143 oxygen in the surface layer was generally high (>6 mg/L), while was low in the bottom. The difference of nitrate  
144 concentration between the model results and in-situ data was relatively obvious. The reason may be that the river  
145 input of nitrate was monthly average in the model.

146 The distribution of dissolved oxygen adjacent to the Yangtze Estuary in September 2010 was showed in Fig.5.  
147 On the whole, it presented that the distribution of dissolved oxygen was high in the north and low in the south. A  
148 closed area with oxygen level less than 2.0 mg/L was appeared off Yangtze Estuary, and was extended along the  
149 Yangtze Estuary to the Zhejiang coastal water. The model results of dissolved oxygen were similar to that  
150 observed by Liu (2012).

151 Model validation results showed that the model can reproduce the variations of biological variables and the  
152 hypoxia in summer at the bottom of the Yangtze Estuary in a certain extent. There were some deviations from the  
153 observed results in some areas, which could due to the complex biogeochemical cycle, parameterization, physical  
154 field and so on. At least, it's suggested that the model can capture some basic conditions of the key physical and



155 biological processes in the Yangtze Estuary, which is helpful for further exploring the mechanism of the formation  
156 of hypoxia off the Yangtze Estuary.

### 157 **3.2 The impacts of river discharge on hypoxia**

158 To evaluate the role of the seasonal variation in river discharge on the hypoxic area, we conducted a  
159 sensitivity experiment (denoted as ‘Qconst’) where river discharge was set to the annual mean value for 2010 and  
160 the other conditions were the same as the Base model run (Table 1). The extent of hypoxic water off the Yangtze  
161 Estuary can be quantified by calculating the total area of water that has bottom dissolved oxygen concentrations  
162 below different threshold value (1.0 mg/L, 2.0 mg/L, 3.0 mg/L). If there was no special note, the hypoxic area was  
163 denoted as the area of DO<2 mg/L in this paper. In the Base model run, hypoxia zone was first appeared off the  
164 Yangtze Estuary in July, then reached its peak in August and September, finally it was reduced and gradually  
165 disappeared in October (Fig.6a). The results were consistent with the findings of previous work conducted by Wei  
166 (2015). As shown in Fig. 6a, the seasonal variations in hypoxic area in the Qconst run were almost consistent with  
167 the Base model run, which suggested that the seasonal variation of hypoxic area was not remarkably affected by  
168 the temporal variation of the river discharge of Yangtze River. In addition, the area of the bottom dissolved  
169 oxygen concentration less than 1 mg/L, 2 mg/L and 3 mg/L decreased by 32%, 46%, 19% (Table 2) in the Qconst  
170 run. Next, to evaluate the role of magnitude of river discharge, we conducted Q2 and Q0.5 sensitivity experiments  
171 where the temporal variation in river discharge was preserved but the magnitude was doubled or halved,  
172 respectively for 2010. Doubling the river discharge increased nearly 7 times of the area where the bottom  
173 dissolved oxygen concentration was below the minimum threshold (1 mg/L). A reduction in the river discharge by  
174 50% decreased the total integrated hypoxic area by 20% to nearly 63% under different threshold values.

175 Water stratification prevented the vertical exchange of dissolved oxygen, and it was an essential condition for  
176 the formation of hypoxia. In this paper, Frequency Brunt-Vaisala ( $N^2$ ) was calculated to quantify the stratification  
177 strength, and it was denoted as the stratification strength between the surface and bottom water (Goni et al., 2006).  
178 The greater the  $N^2$ , the stronger stratification of the water was. The calculating area of  $N^2$  was showed in Fig. 1c  
179 of the red rectangle.

$$180 \quad N^2 = -\frac{g}{\rho} \frac{\partial \rho}{\partial z}$$

181 As shown in Fig. 6b, the stratification of water adjacent to the Yangtze Estuary had a significant relationship with  
182 the river discharge. Doubling the river discharge increased markedly the stratification strength, while reducing the  
183 discharge to 50% of the Base model run led to a significant decrease in the stratification. Fig. 7 showed the  
184 correlation of concentration between the bottom dissolved oxygen and the  $N^2$ . We could found that  $N^2$  was



185 inversely proportional to the concentration of bottom dissolved oxygen. The stronger the stratification, the lower  
186 concentration of bottom dissolved oxygen. The absolute values of correlation coefficient were higher than 0.6, and  
187 the maximum of absolute correlation coefficient was 0.73 in the Q2 run.

### 188 **3.3 The impacts of wind forcing on hypoxia**

189 The wind forcing also had a significant effect on the occurrence and development of hypoxia. Increasing  
190 wind speed enhanced the vertical mixing of water, and promoted the vertical exchange of dissolved oxygen, which  
191 would lead to break the formation of hypoxia (Scully, 2010b). The Yangtze Estuary is mainly controlled by the  
192 East Asian monsoon. The wind speed and wind direction have obvious seasonal variability over the Yangtze  
193 Estuary, namely low magnitude and dominantly southerly direction in summer (July to September) and relatively  
194 high magnitude and northerly direction in winter. In order to evaluate the role of seasonal changes in wind forcing,  
195 we conducted wind runs where the August wind (denoted as ‘WAug’) and January wind (denoted as ‘WJan’) was  
196 repeated each month of 2010, respectively. By forcing the model in this way, the winds had daily variations  
197 associated with the passage of weather systems, but the seasonal variation of speed and direction were removed.  
198 Although this kind of situation did not exist in practice, it was helpful for us to further understand the impacts of  
199 wind forcing on hypoxia. The seasonal variability of wind speed and direction had a great impact on the seasonal  
200 cycle of the simulated hypoxic area. When strong, northerly winds in January were repeated all year in the WJan  
201 run, the hypoxia off the Yangtze Estuary was nearly disappeared. In contrast, when in the WAug run where light,  
202 southerly wind conditions were repeated all year, the hypoxia was extensive from July to October (Fig. 10a), and  
203 the integrated hypoxic area ( $DO < 2$  mg/L) increased roughly 25% compared to the Base model run (Table 2).  
204 Hypoxic area also showed obvious seasonal changes. Hypoxic area was the largest in summer, while essentially  
205 no hypoxia was simulated in the other months. Possible reason was that the phytoplankton was affected by water  
206 temperature, and decreased in early spring and winter, so that the consumption of dissolved oxygen was reduced  
207 due to organic matter decomposition.

208 To further examine the effects of wind speed on the hypoxia, we conducted a ‘W0.9’ wind run where the  
209 wind speed decreased 10%, and a ‘W1.1’ wind run where the wind speed increased by 10% during the summer  
210 (July to September). The magnitude of summer wind speed had a significant impact on the hypoxic area off the  
211 Yangtze Estuary. When summer wind speed decreased, the integrated hypoxic area was increased by roughly 45%.  
212 While increasing in summer wind speed led to a reduction by nearly 64% of hypoxic area (Table 2).

213 Previous study had suggested that hypoxic area was also sensitive to wind direction (Scully, 2010a; Xia and  
214 Jiang, 2015). To further evaluate the influence of wind direction on the hypoxia, we conducted the model runs  
215 where summer wind direction (July to September) were systematically varied in the model forcing. As is typical



216 in most summers, the wind during the 2010 summer is predominately from the south. In the wind direction  
217 sensitivity runs, the modeled wind forcing during the summer (July to September) was rotated by  $180^\circ$  (W180 $^\circ$ ),  
218 negative  $90^\circ$  (W -  $90^\circ$ ), and positive  $90^\circ$  (W +  $90^\circ$ ), resulting in model forcing had the summer winds from the  
219 north, east, and west, respectively (Table 1). Although these simulations were not realistic, they provide insights  
220 into the impacts of wind direction on the hypoxia. When the summer wind direction was from the north (W180 $^\circ$ ),  
221 the integrated hypoxic area off Yangtze Estuary was the minimum, and reduced by nearly 30% compared with  
222 Base model run. The integrated hypoxic area was greatest when the summer wind came from the west (W +  $90^\circ$ ),  
223 and it was increased by nearly 20%. The summer wind direction from the east (W- $90^\circ$ ) led to a reduction by nearly  
224 10% of the integrated hypoxic area (Table 2).

225

## 226 4. Discussion

### 227 4.1 River discharge

228 Stratification was an important indicator of oxygen concentration in bottom water, which prevented the  
229 exchange of dissolved oxygen from the surface to bottom, eventually resulting in hypoxia in the bottom water  
230 (Rabouille et al., 2008). The simulated seasonal cycle of hypoxic area on the Qconst run was similar to the Base  
231 model run (Fig. 6a), which suggested that the temporal variation in river discharge was not an important factor  
232 controlling the seasonal cycle of hypoxic area. But the magnitude of Yangtze River discharge variation could lead  
233 to significant changes on the hypoxic area. Increasing river discharge led to an expansion of the lighter, fresher  
234 river plume water offshore and an enhancement of stratification (Fig. 8a), which limited the effective supplement  
235 of surface high dissolved oxygen. This result consequently caused a reduction of bottom dissolved oxygen  
236 (Fig.8c). And the integrated hypoxic area was increased by 92%, the lowest value of bottom dissolved oxygen  
237 from the Base model run of 1.11 mg/L, reduced to 0.78 mg/L. Whereas decreasing river discharge reduced the  
238 stratification, and thereby significantly increased the vertical oxygen flux through the pycnocline. As a result, the  
239 integrated hypoxic area decreased by 55% and the lowest value of bottom dissolved oxygen increased to 1.32  
240 mg/L. This findings were consistent with the results of previous work conducted by Scully (2013). In addition,  
241 there was a significant negative correlation between the bottom dissolved oxygen and the stratification (Fig. 7).  
242 When the water stratification was strong, the bottom dissolved oxygen was low. While the water stratification was  
243 weak, and the bottom dissolved oxygen was high. Fig. 8a further showed that doubling or halving the river  
244 discharge respectively enhanced or reduced stratification over the majority of the shelf in summer months,  
245 resulting in decrease or increase the bottom dissolved oxygen.

246 Increasing river discharge leaded to offshore extension of the fresher river plume water (Fig.9b), bringing





247 rich nutrients to the eastward. As a result, surface chlorophyll over the majority of the eastern shelf was increased  
248 in Q2 run relative to the Base model run (Fig.8b), which caused the continuous decrease in oxygen level at the  
249 lower layer through decomposition of organic matters. In contrast, decreasing the river discharge confined the  
250 river plume water to near the river mouths (Fig.9c), which limited the nutrients to eastward. As seen in Fig 8b,  
251 surface chlorophyll was decreased over the majority of the shelf in Q0.5 run compared to the Base model run.  
252 Thus, bottom dissolved oxygen was increased and hypoxic zone was decreased, due to the decomposition of  
253 organic matters was reduced in the bottom water.

#### 254 **4.2 Wind Forcing**

255 Strong wind could trigger strong vertical mixing and promote the vertical exchange of dissolved oxygen,  
256 which broke the formation of hypoxia (Chen et al., 2014; Ni et al., 2014). Our simulated results showed that the  
257 variation in wind speed and direction significantly influence the stratification and hence the hypoxic area. In the  
258 WJan wind run, the strong wind homogenized the water column, reducing stratification and producing essentially  
259 no hypoxia throughout the year. Fig. 11a showed that  $N^2$  was negative in the most areas, except in the eastern part  
260 of the Hangzhou bay, which suggested that the water mixing was strong and the vertical flux of dissolved oxygen  
261 increased in WJan wind run. As a result, the bottom dissolved oxygen concentration was increased (Fig. 11c), and  
262 there was almost no hypoxia in the bottom water off the Yangtze Estuary in WJan wind run. In addition, the  
263 strong northwest wind in January resulted in strong estuarine residual velocities that brought the high dissolved  
264 oxygen from the north of Yellow Sea to Yangtze River Estuary. Therefore, even though the average stratification  
265 strength in WJan wind run was stronger than the Q0.5 run (Table 2), WJan nearly did not develop any hypoxia  
266 throughout the year. From the Fig.11b, it could be seen that the surface chlorophyll concentration of WJan wind  
267 run was significantly lower than the Base model run. The possible reason was that the strong wind from northwest  
268 in WJan wind run drove downwelling due to Ekman dynamics, which made the concentration of surface  
269 chlorophyll decreased, and ultimately led to an enhancement of dissolved oxygen through lower decomposition of  
270 organic matters. These finds were the same as the results reported in the study conducted in the northern Gulf of  
271 Mexico shelf by Feng (2014).Above all the reasons, in the WJan wind run there was almost no hypoxia in the  
272 summer adjacent the Yangtze River Estuary.

273 In contrast, in the WAug wind run, the persistently weak wind enhanced the stratification and reduced the  
274 vertical flux of dissolved oxygen, resulting in decreasing bottom dissolved oxygen and promoting widespread  
275 hypoxia. In addition, the concentration of surface chlorophyll was increased adjacent to Yangtze Estuary and  
276 along the coast of Zhejiang in the WAug wind run (Fig. 11b). This result suggested that bottom dissolved oxygen  
277 declined with the decomposition of organic matters.



278 Simulations of hypoxic area showed significant variability in the response to wind speed. In the W1.1 wind  
279 run, the increase in wind speeds was thought to play a key role in breaking down stratification and increasing the  
280 vertical flux of dissolved oxygen. Increased wind speeds generally raised bottom dissolved oxygen concentration  
281 (Fig. 11c). This finding was similar to the results conducted in the Louisiana Coasts, where the authors suggested  
282 that wind-induced vertical mixing could result in significant reductions in the hypoxic area (Wiseman et al., 1997).  
283 As shown in Fig. 11b, in the area of 28-32°N 122-123.5°E, decreased surface chlorophyll resulted in lower  
284 dissolved oxygen consumption, which increased the dissolved oxygen in the bottom water. In contrast, in the  
285 W0.9 wind run, the dissolved oxygen flux from the upper layers due to stronger stratification was reduced. And  
286 increased surface chlorophyll concentration on the north of 30° led to huge dissolved oxygen consumption caused  
287 by the decay of dead phytoplankton (Fig.11b). These results worked together to decrease the bottom dissolved  
288 oxygen and create hypoxic expansion. Scully (2013) illustrated how changes in wind associated with stratification  
289 and thereby hypoxia on the shelf. They found that increased wind speed decreased the hypoxic area, whereas  
290 decreased wind speed facilitated hypoxia development. These findings were consistent with our results.

291 Changes in wind direction also significantly influence the hypoxic area off Yangtze Estuary. As seen in Fig.  
292 12a, when the mean summer wind direction was from north (W180°), stratification was decreased in the north of  
293 31°N and along the coast of Zhejiang relative to the Base model run. This would lead to an enhancement of  
294 vertical dissolved oxygen flux. Whereas near to the Hangzhou bay, the vertical dissolved oxygen flux was reduced  
295 associated with increased water stratification, resulting in decreased bottom dissolved oxygen (Fig. 12c). Under the  
296 control of the northerly wind (W180°), Zhejiang coastal current was enhanced, bringing the high dissolved oxygen  
297 from the north of Yellow Sea to the Yangtze Estuary. This further led to increased bottom dissolved oxygen off  
298 Yangtze Estuary. From the Fig. 12b, it can be seen that surface chlorophyll concentration in the W180° was lower  
299 than the Base model run. We attributed this to the fact that wind from the north drive downwelling due to Ekman  
300 dynamics. Decreased dissolved oxygen consumption was caused by the reduced decay of dead phytoplankton.  
301 When the summer wind was from the East (W-90°), the average water stratification was similar to the W180°  
302 wind run, but the integrated hypoxic area in W-90° wind run was larger than the W180°. This may be related to  
303 the horizontal distribution of chlorophyll concentration. As shown in Fig. 12b, surface chlorophyll concentration  
304 was higher in W-90° wind run than the W180° run, which would lead to more dissolved oxygen consumption  
305 caused by organic matter decomposition in W-90°. When the summer wind was from the west (W+90°),  
306 stratification was the strongest in the three wind direction runs. And integrated hypoxic area also reached the  
307 maximum. There can be three reasons. For the first reason, Fig. 12a showed that stratification was stronger in the  
308 most areas, except in the north of the 31.5°N relative to the Base model run, which suggested that in most areas



309 the water mixing was weak and the vertical flux of dissolved oxygen reduced. For the second reason, under the  
310 influence of the westerly wind, the residual flow would transport the low dissolved oxygen from the trough off the  
311 Yangtze Estuary to the eastward. For the third reason, from Fig. 12b, it can be found an area of relatively high  
312 chlorophyll concentration off Yangtze Estuary in W+90° wind run. This may be due to Yangtze River which was  
313 rich in nutrients expand to the eastward under the controlling of westerly wind. As a result, it would promote the  
314 growth of phytoplankton. The decomposition of dead phytoplankton was another important factor for the  
315 decreased bottom dissolved oxygen. These reasons work together to create hypoxic conditions.

316

## 317 5. Conclusions

318

319 In this study, a three-dimensional coupled physical-biological model was used to analyze the hypoxia off to  
320 the Yangtze Estuary. This study highlighted that river discharge, wind speed and wind direction all had significant  
321 impacts on the hypoxia. The seasonal cycle of hypoxia was relatively insensitive to the temporal variability in  
322 river discharge. But the integrated hypoxic area was very sensitive to the magnitude of river discharge. Increasing  
323 in the magnitude of river discharge led to enhance stratification, promote the growth of phytoplankton associated  
324 with higher nutrients, and thereby greatly increased hypoxic area off the Yangtze Estuary. In contrast, decreased  
325 in the magnitude of river discharge reduced the stratification and surface chlorophyll concentration and hence  
326 significantly decreased the hypoxic area.

327 Model simulations demonstrated that wind speed and wind direction not only play an important role in the  
328 seasonal cycle of hypoxia, but also in the integrated the hypoxic area. When the winds in January were repeated  
329 all year, the hypoxic zone was nearly disappeared as the result of the strong water mixing induced by strong,  
330 northerly winds. While persistently weak winds from August enhanced stratification and facilitated hypoxia  
331 development. Increasing wind speed weakened stratification and chlorophyll-a concentration, hence decreased the  
332 hypoxic area, while decreasing wind speed did the opposite. Wind direction significantly influenced the extent of  
333 hypoxia. Among the directions runs, the integrated hypoxic area was greatest when the summer wind came from  
334 the west (W + 90°), which was enhanced by nearly 20%. When the summer wind direction was from the north  
335 (W180°), the integrated hypoxic area off Yangtze Estuary was minimum. The integrated hypoxic area reduced by  
336 nearly 10% when the wind was from the east (W-90°).

337 The model did not include inorganic phosphorus and therefore assumed that primary production was limited  
338 by light and nitrogen only. In future studies, the model needs to consider the dynamics of inorganic phosphorus. In  
339 addition, increasing the number of monitoring cruises per year and setting up additional long-term moorings in the



340 East China Sea would be useful to further validate biogeochemical variables and environmental factors.

341

342

### 343 **References**

344 Chapman, D. C.: Numerical treatment of cross-shelf open boundaries in a barotropic coastal ocean model, *Journal of*  
345 *Physical oceanography*, 15, 1060-1075, 1985.

346 Chen, J., Ni, X., Liu, M., Chen, J., Mao, Z., Jin, H., and Pan, D.: Monitoring the occurrence of seasonal low-oxygen  
347 events off the Changjiang Estuary through integration of remote sensing, buoy observations, and modeling, *Journal*  
348 *of Geophysical Research: Oceans*, 119, 5311-5322, 10.1002/2014jc010333, 2014.

349 Diaz, R. J.: Overview of hypoxia around the world, *J Environ Qual*, 30, 275-281, 2001.

350 Feng, Y., Fennel, K., Jackson, G. A., DiMarco, S. F., and Hetland, R. D.: A model study of the response of hypoxia to  
351 upwelling-favorable wind on the northern Gulf of Mexico shelf, *Journal of Marine Systems*, 131, 63-73,  
352 10.1016/j.jmarsys.2013.11.009, 2014.

353 Fennel, K., Hu, J., Laurent, A., Marta-Almeida, M., and Hetland, R.: Sensitivity of hypoxia predictions for the northern  
354 Gulf of Mexico to sediment oxygen consumption and model nesting, *Journal of Geophysical Research: Oceans*, 118,  
355 990-1002, 10.1002/jgrc.20077, 2013.

356 Flather, R.: A tidal model of the northwest European continental shelf, *Mem. Soc. Roy. Sci. Liege, Ser. 6*, 10, 141-164,  
357 1976.

358 Goni, M., Gordon, E., Monacci, N., Clinton, R., Gisewhite, R., Allison, M., and Kineke, G.: The effect of Hurricane Lili  
359 on the distribution of organic matter along the inner Louisiana shelf (Gulf of Mexico, USA), *Continental Shelf*  
360 *Research*, 26, 2260-2280, 10.1016/j.csr.2006.07.017, 2006.

361 Gu, H.: The maximum value of dissolved oxygen in its vertical distribution in Yellow SEA, *Acta Oceanologica Sinica*,  
362 1980.

363 Haidvogel, D. B., Arango, H., Budgell, W. P., Cornuelle, B. D., Curchitser, E., Di Lorenzo, E., Fennel, K., Geyer, W. R.,  
364 Hermann, A. J., and Lanerolle, L.: Ocean forecasting in terrain-following coordinates: Formulation and skill  
365 assessment of the Regional Ocean Modeling System, *Journal of Computational Physics*, 227, 3595-3624, 2008.

366 Karlson, K., Rosenberg, R., Bonsdorff, E., Gibson, R., Barnes, M., and Atkinson, R.: Temporal and spatial large-scale  
367 effects of eutrophication and oxygen deficiency on benthic fauna in Scandinavian and Baltic waters - A review,  
368 *Oceanography and Marine Biology*, Vol 40, 40, 427-489, 2002.

369 Katja Fennel, J. W., Julia Levin, John Moisan: Nitrogen cycling in the Middle Atlantic Bight: Results from a  
370 three-dimensional model and implications for the North Atlantic nitrogen budget, *GLOBAL BIOGEOCHEMICAL*  
371 *CYCLES*, 20, GB3007, 2006.

372 Lewis, M. R., Cullen, J. J., and Platt, T.: Phytoplankton and thermal structure in the upper ocean: consequences of  
373 nonuniformity in chlorophyll profile, *Journal of Geophysical Research: Oceans (1978–2012)*, 88, 2565-2570, 1983.

374 Li, H., Chen, J., Lu, Y., Jin, H., Wang, K., and Zhang, H.: Seasonal variation of DO and formation mechanism of bottom  
375 water hypoxia of Changjiang River Estuary, *Journal of Marine Sciences*, 29, 78-87, 2011.

376 Liu, K.-K., Chao, S.-Y., Lee, H.-J., Gong, G.-C., and Teng, Y.-C.: Seasonal variation of primary productivity in the East  
377 China Sea: A numerical study based on coupled physical-biogeochemical model, *Deep Sea Research Part II: Topical*  
378 *Studies in Oceanography*, 57, 1762-1782, 10.1016/j.dsr2.2010.04.003, 2010.



- 379 Liu Xincheng, S. H., Huang Qinghui: Concentration variation and flux estimation of dissolved inorganic nutrient from  
380 the Changjiang River, *Chinese Journal of Oceanology and Limnology*, 33, 332-340, 2002.
- 381 Liu Zhiguo, X. R., Liu Caicai, Qin Yutao, Cai Peng: Characters of hypoxia area off the Yangtze River Estuary and its  
382 influence, *Marine science bulletin*, 31, 588-593, 2012.
- 383 Marchesiello, P., McWilliams, J. C., and Shchepetkin, A.: Open boundary conditions for long-term integration of  
384 regional oceanic models, *Ocean modelling*, 3, 1-20, 2001.
- 385 Mellor G., T. Y.: Development of a turbulence closure model for geophysical fluid problems, *Geophys.*, 20, 851-875,  
386 1982.
- 387 Morel, A., and Berton, J. F.: Surface pigments, algal biomass profiles, and potential production of the euphotic layer:  
388 Relationships reinvestigated in view of remote - sensing applications, *Limnology and Oceanography*, 34,  
389 1545-1562, 1989.
- 390 Murphy, R. R., Kemp, W. M., and Ball, W. P.: Long-Term Trends in Chesapeake Bay Seasonal Hypoxia, Stratification,  
391 and Nutrient Loading, *Estuaries & Coasts*, 34, 1293-1309, 2011.
- 392 Ni, X., Huang, D., Zeng, D., Zhang, T., Li, H., and Chen, J.: The impact of wind mixing on the variation of bottom  
393 dissolved oxygen off the Changjiang Estuary during summer, *Journal of Marine Systems*, 2014.
- 394 Ning, X., Lin, C., Su, J., Liu, C., Hao, Q., and Le, F.: Long-term changes of dissolved oxygen, hypoxia, and the  
395 responses of the ecosystems in the East China Sea from 1975 to 1995, *Journal of Oceanography*, 67, 59-75, 2011.
- 396 Obenour, D. R., A. Michalak, and D. Scavia: Assessing biophysical controls on Gulf of Mexico hypoxia through  
397 probabilistic modeling, *Ecological Applications*, 25, 492-505, 2015.
- 398 Rabouille, C., Conley, D. J., Dai, M. H., Cai, W. J., Chen, C. T. A., Lansard, B., Green, R., Yin, K., Harrison, P. J., Dagg,  
399 M., and McKee, B.: Comparison of hypoxia among four river-dominated ocean margins: The Changjiang (Yangtze),  
400 Mississippi, Pearl, and Rhône rivers, *Continental Shelf Research*, 28, 1527-1537, 10.1016/j.csr.2008.01.020, 2008.
- 401 Scully, M. E.: Wind Modulation of Dissolved Oxygen in Chesapeake Bay, *Estuaries and Coasts: J ERF*, 33, 1164-1175,  
402 10.1007/s12237-010-9319-9, 2010a.
- 403 Scully, M. E.: The Importance of Climate Variability to Wind-Driven Modulation of Hypoxia in Chesapeake Bay,  
404 *Journal of Physical Oceanography*, 40, 1435-1440, 10.1175/2010jpo4321.1, 2010b.
- 405 Scully, M. E.: Physical controls on hypoxia in Chesapeake Bay: A numerical modeling study, *Journal of Geophysical*  
406 *Research: Oceans*, 118, 1239-1256, 10.1002/jgrc.20138, 2013.
- 407 Shchepetkin A F, M. J. C.: The regional oceanic modeling system(ROMS): a split—explicit, free—surface,  
408 topography-following-coordinate oceanic model, *Ocean Modelling*, 9, 347-404, 2005.
- 409 Vaquer-Sunyer, R., and Duarte, C.: Thresholds of hypoxia for marine biodiversity, *Proceedings of the National*  
410 *Academy of Sciences of the United States of America*, 105, 15452-15457, 10.1073/pnas.0803833105, 2008.
- 411 Wang, B.: Hydromorphological mechanisms leading to hypoxia off the Changjiang estuary, *Marine Environmental*  
412 *Research*, 67, 53-58, 10.1016/j.marenvres.2008.11.001, 2009.
- 413 Wei, H., He, Y., Li, Q., Liu, Z., and Wang, H.: Summer hypoxia adjacent to the Changjiang Estuary, *Journal of Marine*  
414 *Systems*, 67, 292-303, 10.1016/j.jmarsys.2006.04.014, 2007.
- 415 Wei, Q., Wang, B., Chen, J., Xia, C., Qu, D., and Xie, L.: Recognition on the forming-vanishing process and underlying  
416 mechanisms of the hypoxia off the Yangtze River estuary, *Science China Earth Sciences*, 58, 628-648, 2015.



417 Wilson, R. E., Swanson, R. L., and Crowley, H. A.: Perspectives on long-term variations in hypoxic conditions in  
418 western Long Island Sound, *Journal of Geophysical Research*, 113, 10.1029/2007jc004693, 2008.

419 Wiseman, W. J., Rabalais, N. N., Turner, R. E., Dinnel, S. P., and Macnaughton, A.: Seasonal and interannual variability  
420 within the Louisiana coastal current: stratification and hypoxia, *Journal of Marine Systems*, volume 12, 237-248,  
421 1997.

422 X Li, Z. Y., X Song, X Cao: The seasonal characteristics of dissolved oxygen distribution and hypoxia in the  
423 Changjiang Estuary, *Journal of Coastal Research*, 27, 2011.

424 Xia, M., and Jiang, L.: Influence of wind and river discharge on the hypoxia in a shallow bay, *Ocean Dynamics*, 65,  
425 665-678, 10.1007/s10236-015-0826-x, 2015.

426 Yin, K., Lin, Z., and Ke, Z.: Temporal and spatial distribution of dissolved oxygen in the Pearl River Estuary and  
427 adjacent coastal waters, *Continental Shelf Research*, 24, 1935–1948, 2004.

428 Zhou F, H. D., Ni X: Hydrographic analysis on the multi-time scale variability on hypoxia adjacent to the Changjiang  
429 River estuary, *Acta Ecol Sin*, 30, 4728-4720, 2010.

430 Zhu, Z.-Y., Zhang, J., Wu, Y., Zhang, Y.-Y., Lin, J., and Liu, S.-M.: Hypoxia off the Changjiang (Yangtze River) Estuary:  
431 Oxygen depletion and organic matter decomposition, *Marine Chemistry*, 125, 108-116,  
432 10.1016/j.marchem.2011.03.005, 2011.

433

434

435

436

437

438

439

440

441

442

443

444

445

446

447

448

449

450

451

452

453

454

455

456

457

458

459



460  
 461  
 462

**Table.1 Model sensitivity experiment**

Experiments	Description
Base model run	
Base	Base run with realistic river discharge and wind forcing in year 2010
River discharge runs	
Qconst	River discharge was set to annual average value
Q2	Double the river discharge
Q0.5	Halve the river discharge
Wind runs	
WJan	Winds from January were repeated for every month of the year
WAug	Winds from August were repeated for every month of the year
W0.9	Summer (July–September) wind magnitude was decreased by 10%
W1.1	Summer (July–September) wind magnitude was increased by 10%
W180°	Summer (July–September) wind direction was rotated 180°
W-90°	Summer (July–September) wind direction was rotated negative 90°
W+90°	Summer (July–September) wind direction was rotated positive 90°

463  
 464  
 465  
 466  
 467

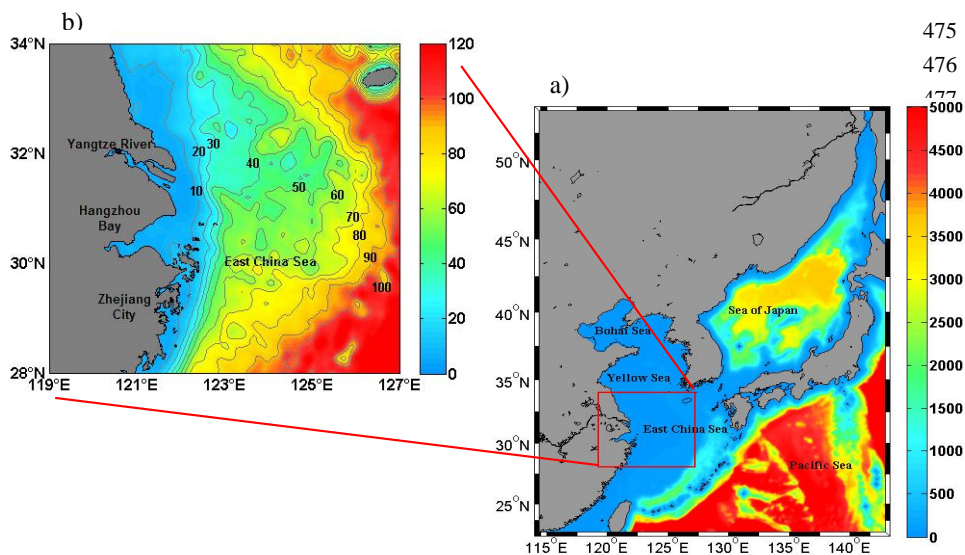
**Table.2** The total area of hypoxia area under different thresholds of DO, and the average N<sup>2</sup> in summer and the year

Experiments	Integrated Hypoxic Area (10 <sup>3</sup> km <sup>2</sup> days)			Average N <sup>2</sup>	
	<1mg/L	<2mg/L	<3mg/L	Summer average	Yearly average
Base model run					
Base	11.7	330.5	1163	5.58×10 <sup>-4</sup>	2.63×10 <sup>-4</sup>
River runs					
Qconst	8.0 (-32%)	179.6 (-46%)	939.3 (-19%)	3.80×10 <sup>-4</sup> (-32%)	2.24×10 <sup>-4</sup> (-15%)
Q2	94.1(+704%)	634.8(+92%)	1640.4(+41%)	10×10 <sup>-4</sup> (+79%)	5.03×10 <sup>-4</sup> (+91%)
Q0.5	4.33 (-63%)	147.1 (-55%)	927.7 (-20%)	3.28×10 <sup>-4</sup> (-41%)	1.59×10 <sup>-4</sup> (-40%)
Wind runs					
WJan	0 (-100%)	13.9 (-96%)	256.8 (-78%)	4.06×10 <sup>-4</sup> (-27%)	1.90×10 <sup>-4</sup> (-28%)
WAug	25.4(+117%)	412.8 (+25%)	1435.3(+23%)	6.25×10 <sup>-4</sup> (+12%)	3.02×10 <sup>-4</sup> (+15%)
W0.9	49.0(+319%)	478.0 (+45%)	1296.8(+12%)	6.29×10 <sup>-4</sup> (+13%)	2.80×10 <sup>-4</sup> (+6%)
W1.1	0 (-100%)	118.9 (-64%)	894.4 (-23%)	4.89×10 <sup>-4</sup> (-12%)	2.45×10 <sup>-4</sup> (-7%)
W180°	13.8 (+18%)	235.5 (-29%)	909.4 (-22%)	4.97×10 <sup>-4</sup> (-11%)	2.45×10 <sup>-4</sup> (-7%)
W-90°	14.6 (+25%)	296 (-10%)	1020.5(-12%)	5.07×10 <sup>-4</sup> (-9%)	2.51×10 <sup>-4</sup> (-5%)
W+90°	20.3 (+74%)	390.9 (+18%)	1240 (+7%)	6.68×10 <sup>-4</sup> (+20%)	2.85×10 <sup>-4</sup> (+8%)

468  
 469  
 470  
 471  
 472



473  
 474



475  
 476  
 491

492  
 493  
 494  
 495  
 496  
 497  
 498  
 499

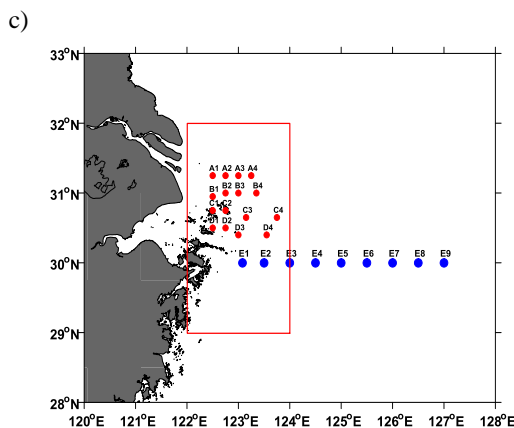


Fig.1 (a) Model domain and depth. Red box is the region of Fig.1b. (b) The model bathymetry (shading map, unit: meter) of East China Sea. (c) Red dots are the station observation in August 2011, blue dots are the section observation in August 2011, the red rectangle indicates the region used for the calculation of  $N^2$ .

500  
 501  
 502  
 503  
 504  
 505  
 506  
 507  
 508  
 509  
 510



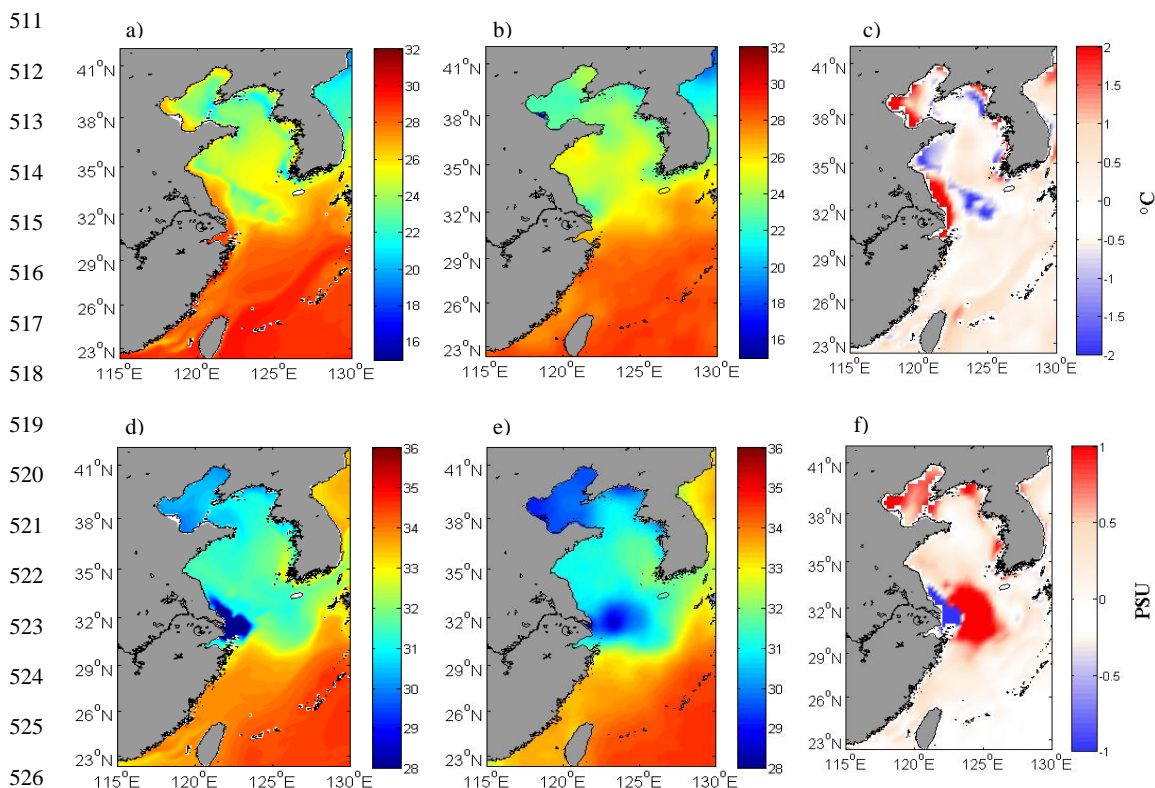
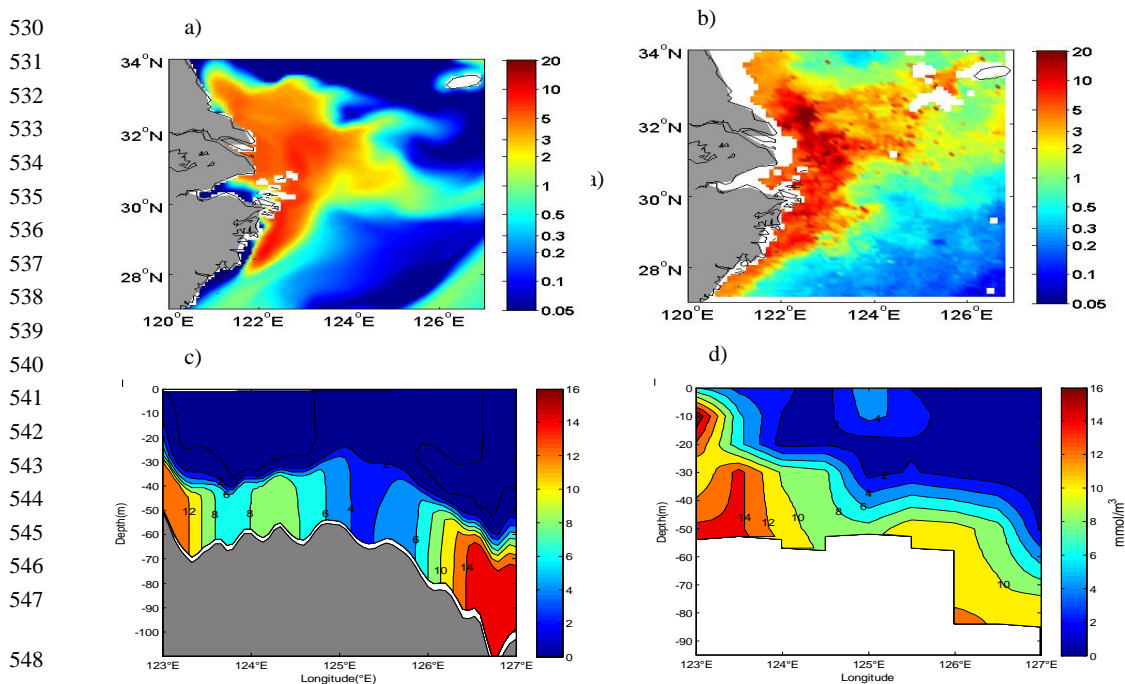
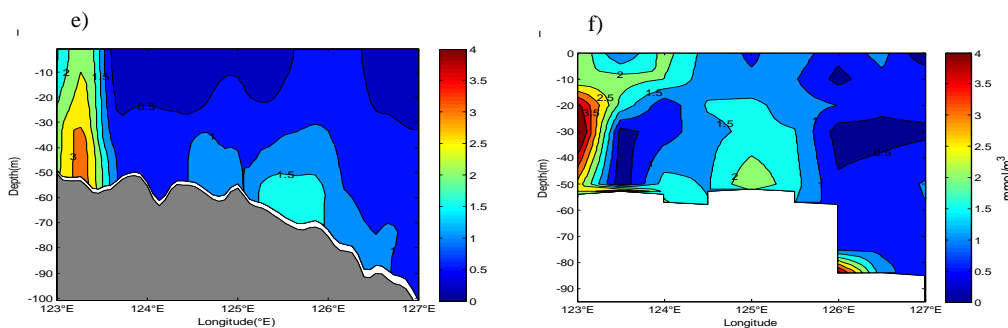


Fig.2 The comparison between modeled results (a) and GDEM data (b) of climatological field of SST in August, and the difference between them (c). The comparison between modeled results (d) and GDEM data (e) of climatological field of SSS in August, and the difference between them (f).



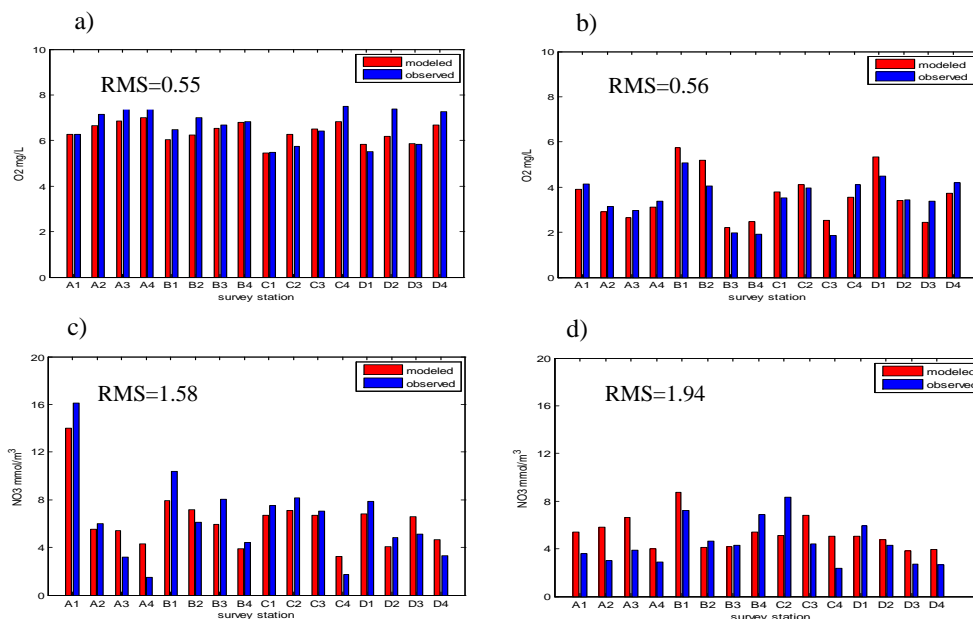


549  
 550  
 551  
 552  
 553  
 554  
 555  
 556  
 557  
 558  
 559



560 Fig.3 The comparison between modeled results (a) and SeaWiFS-derived data (b) of chlorophyll-a concentration in August 2010.  
 561 The comparison between modeled results (c) and in-situ data (d) of NO<sub>3</sub> along the section of 30°N in August 2011. The  
 562 comparison between modeled results (e) and in-situ data (f) of NH<sub>4</sub> along the section of 30°N in August 2011.

563  
 564  
 565  
 566  
 567  
 568  
 569  
 570  
 571  
 572  
 573  
 574



575  
 576  
 577  
 578  
 579  
 580  
 581  
 582  
 583

584 Fig.4 The comparison between modeled results (red bars) and observed data (blue bars) of NO<sub>3</sub> and DO at the stations in August  
 585 2011 (see Figure 1c). (a), (b) Respectively represent the surface DO and bottom DO; (c), (d) Respectively, represent the surface NO<sub>3</sub>  
 586 concentration and bottom NO<sub>3</sub> concentration

587  
 588  
 589  
 590  
 591  
 592  
 593  
 594  
 595



596  
 597  
 598  
 599  
 600  
 601  
 602  
 603  
 604  
 605  
 606  
 607  
 608  
 609  
 610  
 611  
 612  
 613  
 614  
 615  
 616

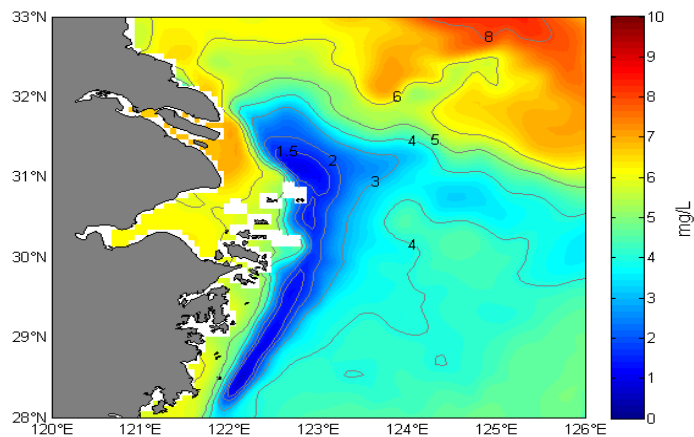


Fig.5 The modeled patterns of hypoxia zone off the Yangtze Estuary in September 2010

617  
 618  
 619  
 620  
 621  
 622  
 623  
 624  
 625

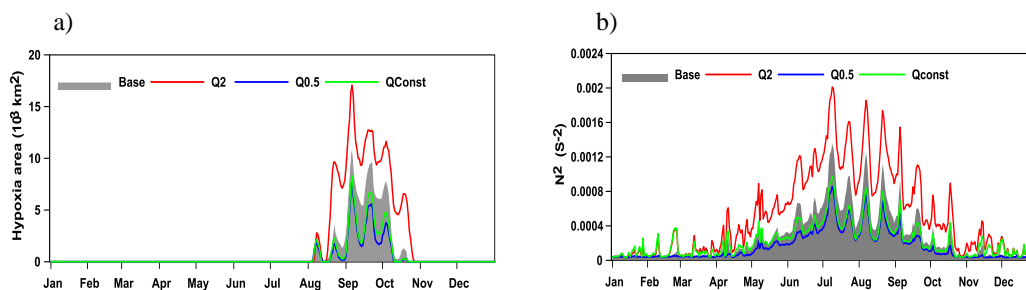


Fig.6 (a), (b) are the hypoxia area ( $DO < 2 \text{ mg/L}$ ) and  $N^2$  in the river discharge experiment, respectively. The gray shaded part represents the Base run and the red, blue, green curve represent Q2, Q0.5, Qconst, respectively.

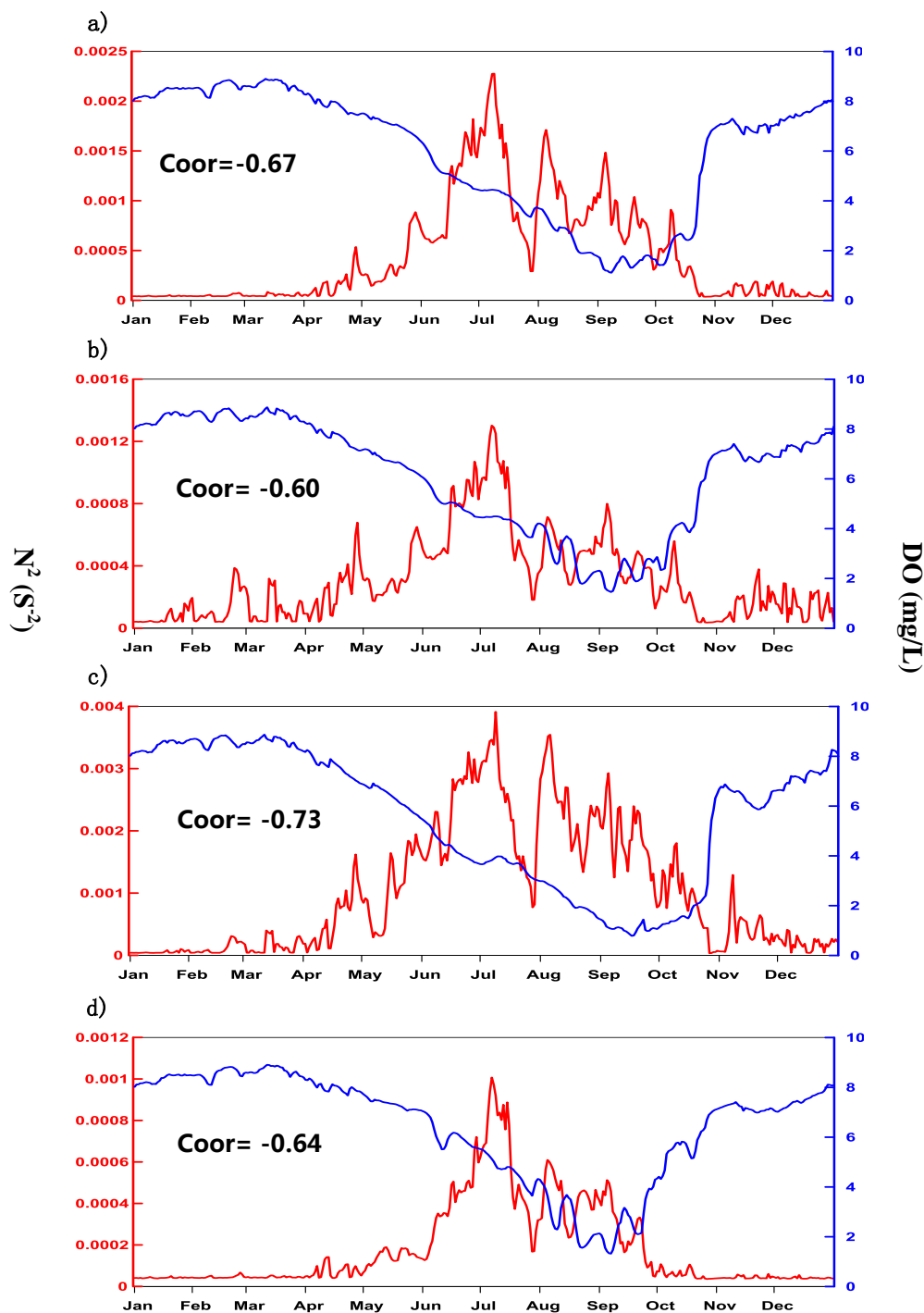


Fig.7 The correlation between the bottom dissolved oxygen concentration and  $N^2$  in the station of  $123^\circ E$ ,  $31^\circ N$ . The blue curve represents the bottom dissolved oxygen concentration, and the red curve represents  $N^2$ . (a), (b), (c), (d) respectively represent the Base run, Qconst, Q2, Q0.5.

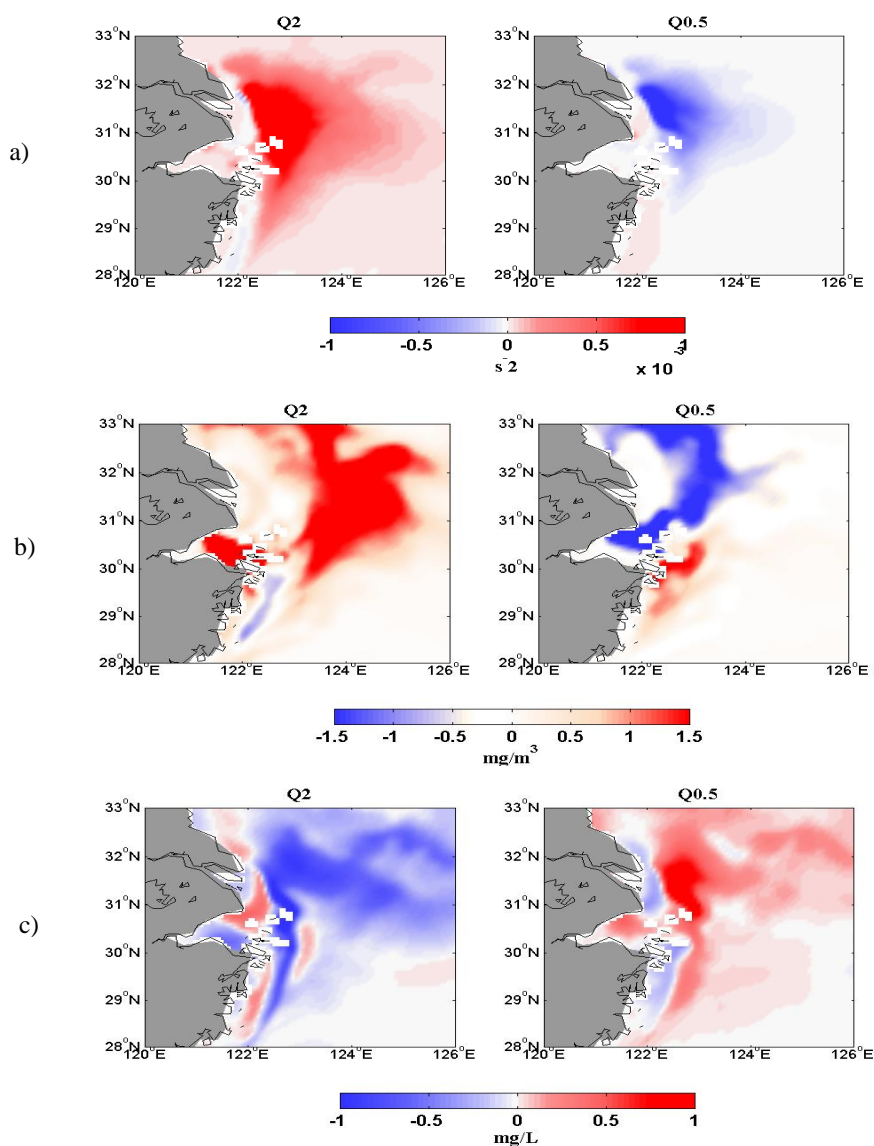


Fig.8 (a) The deviation in summer (7-9 months) stratification( $N^2$ ) of Q2, Q0.5 from the Base run. (b)The deviation in summer (7-9 months) chlorophyll concentration of Q2, Q0.5 from the Base run. (c) The deviation in summer (7-9 months) bottom dissolved oxygen concentration of Q2, Q0.5 from the Base run.

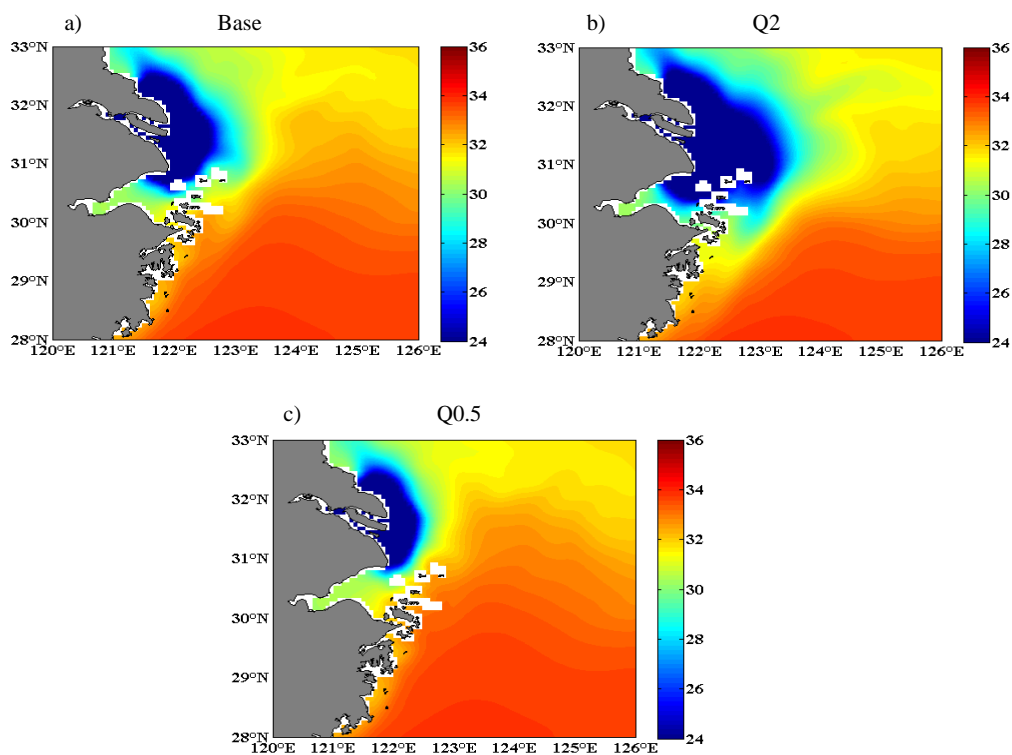


Fig.9 Averaged surface salinity for the period July to September in river runs. (a), (b), (c) respectively represent the Base run, Q2, Q0.5.

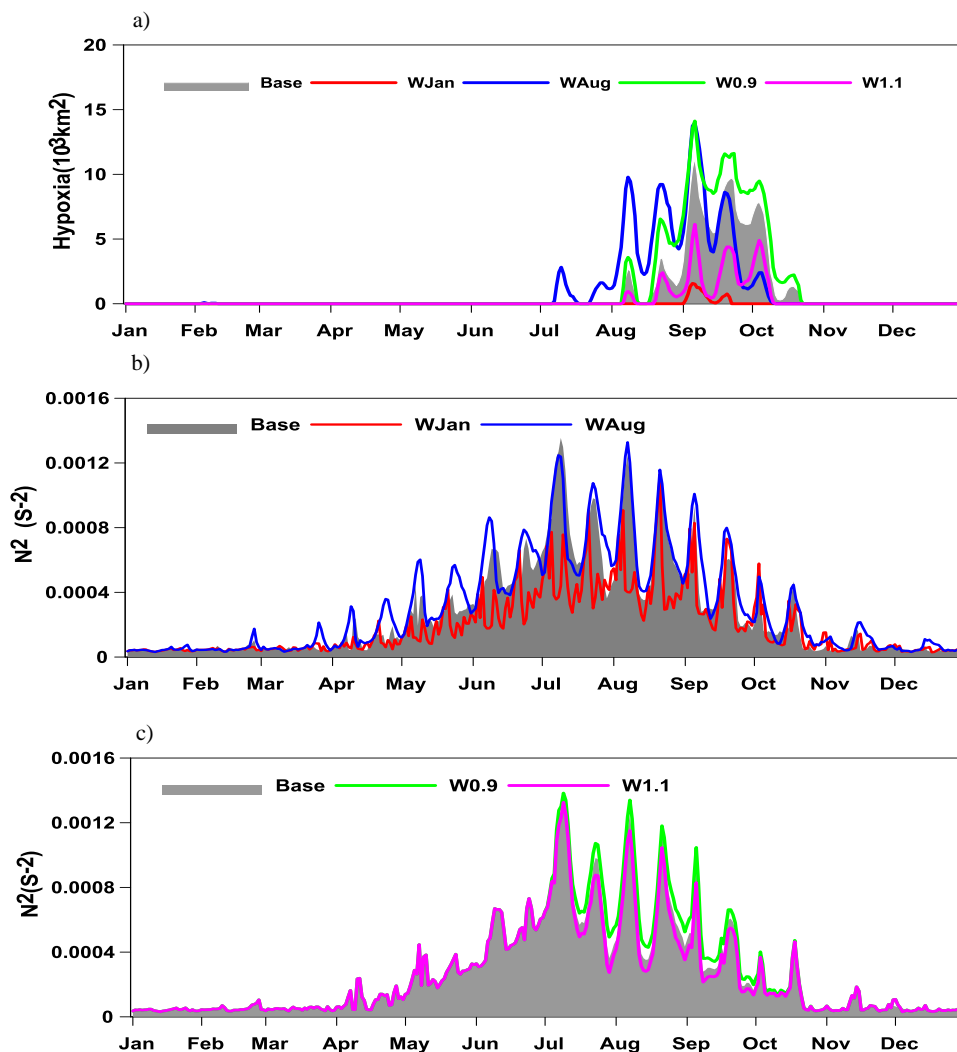


Fig.10 (a) The comparison of the simulated hypoxic area ( $\text{DO} < 2 \text{ mg/L}$ ) on the wind variation runs. (b),(c) Averaged stratification  $N^2$  for the Base run (gray shadow) and wind variation runs

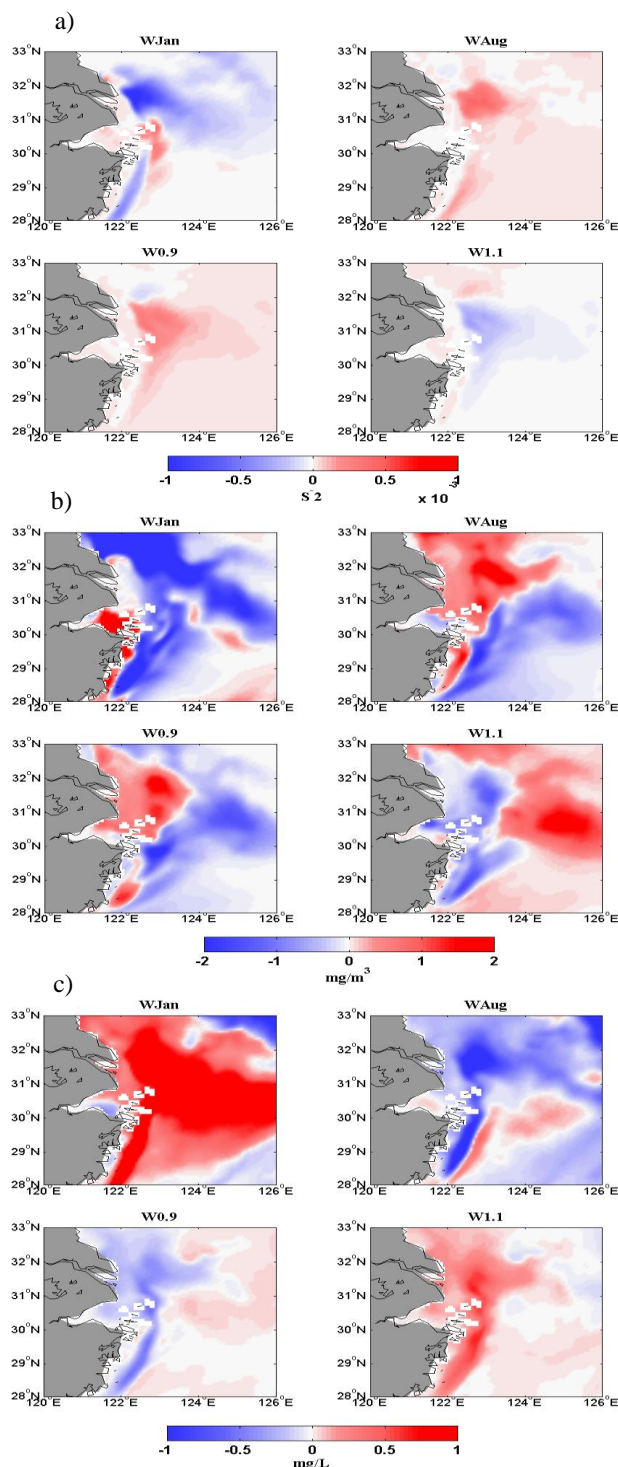


Fig.11 (a) The deviation in summer (7-9 months) stratification( $N^2$ ) of wind variation runs from the Base model. (b) The deviation in summer (7-9 months) chlorophyll concentration of wind variation runs from the Base model. (c) The deviation in summer (7-9 months) bottom dissolved oxygen concentration of wind variation runs from the Base model



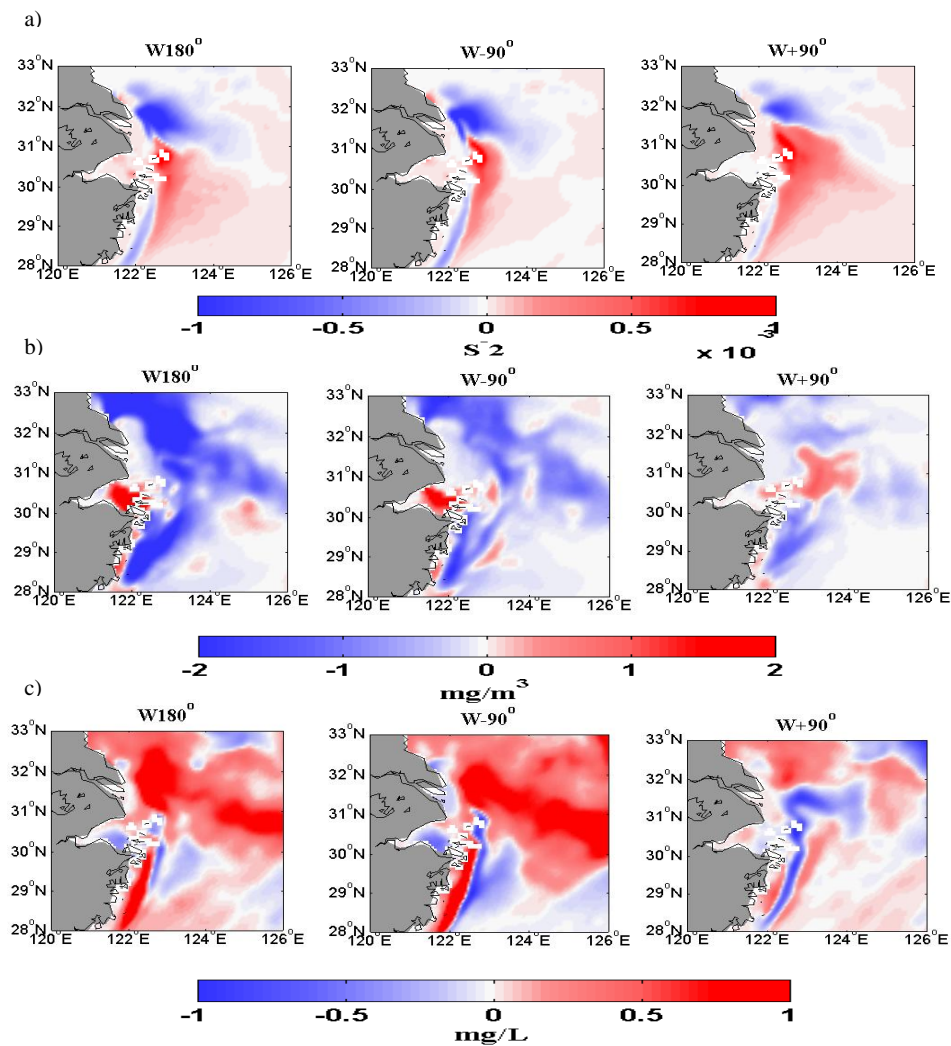


Fig.12 (a) The deviation in summer (7-9 months) stratification( $N^2$ ) of wind direction variation runs from the Base model. (b) The deviation in summer (7-9 months) chlorophyll concentration of wind direction variation runs from the Base model. (c) The deviation in summer (7-9 months) bottom dissolved oxygen concentration of wind direction variation runs from the Base model